JOURNAL OF THEORETICAL AND APPLIED MECHANICS
60, 4, pp. 579-591, Warsaw 2022
https://doi.org/10.15632/jtam-pl/152712

FRACTURE ANALYSIS FOR VISCOELASTIC CREEP USING PERIDYNAMIC FORMULATION

Muhammad A. Azizi, Mohd Z.M. Zahari, Sharafiz A. Rahim, Muhamad A. Azman
Faculty of Engineering and Built Environment, Universiti Kebangsaan Malaysia, Bangi, Malaysia
Corresponding author M.A. Azizi, e-mail: muhdazim@upm.edu.my

The purpose of this paper is to provide a peridynamic (PD) model for the prediction of the viscoelastic creep deformation and failure model. The viscoelastic characteristic consists of several stages, namely primary creep, secondary creep, tertiary creep and fracture. A nonlinear viscoelastic creep equation based on the internal state variable (ISV) theory covering four creep stages and PD equations are used. The viscoelastic equation is inserted into the PD equation to derive a PD model with two time parameters, i.e., numerical time and viscoelastic real time. The parameters of the viscoelastic equation are analyzed and optimized. A comparison between numerical and experimental data is performed to validate this PD model. The new PD model for nonlinear viscoelastic creep behavior is confirmed by an acceptable similarity between the numerical and experimental creep strain curves with an error of 15.85%. The nonlinearity of the experimental and numerical data is sufficiently similar as the error between the experimental and numerical curves of the secondary stage strain rate against the load is 21.83%. The factors for the errors are discussed and the variation of the constants in the nonlinear viscoelastic model is also investigated.

Keywords: viscoelastic, peridynamic, creep behavior, fracture mechanic

1. Introduction

Current practice of viscoelastic creep prediction relies on the finite element method (FEM). The major drawback of the conventional FEM is that it cannot include crack initiation and propagation. It suffers from discontinuous stress and strain fields that require special treatment of singularities. Therefore, this study presents a method for predicting material failure under continuous loading using peridynamic (PD) theory (Silling, 2000; Foster *et al.*, 2009; Hu *et al.*, 2013), which is a significant departure from the generally accepted FEM. This approach accounts for material failure on its own, without the need for external crack growth criteria and post-processing. Failure occurs when and where it is energetically favorable. The PD theory has accurately predicted crack properties in many experimental studies under quasi-static and dynamic loading, such as the brittle fracture pattern (Agwai *et al.*, 2011), crack propagation in multilayered structures (Warren *et al.*, 2009), structural stability (Kilic and Madenci, 2009) and crack branching (Ha and Bobaru, 2011). The PD formulation is applied to viscoelastic creep behavior in this work to further extend the numerical model.

Materials that exhibit both solid-like and fluid-like properties are categorized as viscoelastic materials (Xu and Yuan, 2011). Most biological materials exhibit viscoelastic behavior, e.g., polymers, fibers, tissues such as tendons and ligaments. Some metals exhibit viscoelastic behavior at elevated temperature. Two important tests to describe time-dependent viscoelastic properties are the creep test and the relaxation test. This work contributes to an extension of the PD model through application of the numerical theory on the viscoelastic creep behavior. The application is made by replacing the deformation component in the PD equation with the viscoelastic equation.

2. Peridynamic formulation

In the formulation work, the PD formulation, as given in equation (2.1), is the same as the conventional finite element equation of motion, except for the internal force or bond force equation, i.e., the first component in equation (2.1). The conventional differential component in FEM is replaced by an integral component in PD. The body forces **b** correspond to the conventional equation. This bond force equation has the dimension of force per unit volume F/V

$$\rho\frac{\partial^2\mathbf{u}}{\partial t^2} = \int_R dV_{x'}\mathbf{f}(\mathbf{u}(\mathbf{x},t),\mathbf{u}(\mathbf{x}',t),\mathbf{x},\mathbf{x}',t) + \mathbf{b}(\mathbf{x},t) \tag{2.1}$$

In the PD model, a particle $\mathbf{x}$ interacts only with another particle $\mathbf{x}'$ within the horizon of the particle $\mathbf{x}$, as shown in Fig. 1a. $\mathbf{u}$ is the displacement of all particles. The horizon in the 3-dimensional model has the shape of a sphere. The radius of the horizon R varies between 2 and 3 times the discretization length, where the internal length is the measure of nonlocal behavior, as shown in Eq. (2,2). When R is greater than $3l$, the time required for the process increases, while when R is less than $2l$, the model behaves like in the conventional local continuum mechanics.

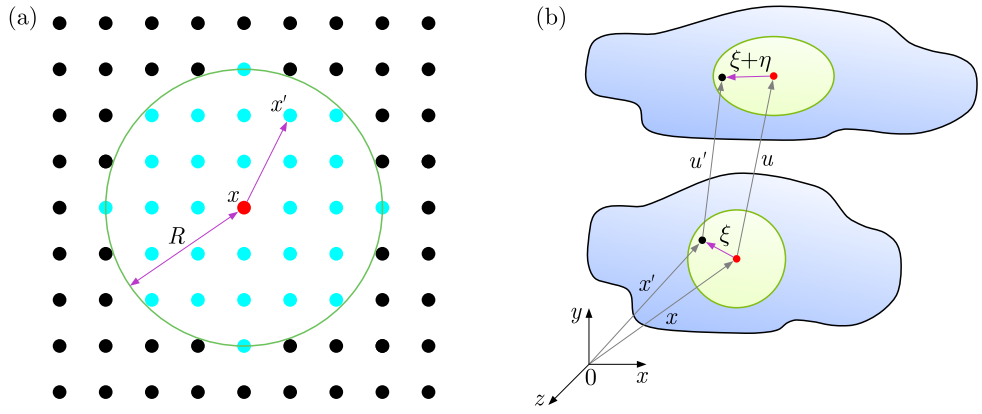

Fig. 1. (a) Horizon of a particle in the PD model. (b) Definition of $\boldsymbol{\xi}$ and $\boldsymbol{\eta}$ in the PD model (Xu and Yuan, 2011)

The component $\mathbf{f}$ is a pairwise force function with a unit force per unit volume squared as stated in Eq. (2.2). It describes the strain behavior of each bond between 2 particles. $\boldsymbol{\eta}$ is the elongation of bonds between nodes, $\boldsymbol{\xi}$ is the initial distance between nodes as shown in Fig. 1b, $\mathbf{s}$ is strain where $\mathbf{s} = \boldsymbol{\eta}/\boldsymbol{\xi}$, and c_1 is the material deformation coefficient (Warren *et al.*, 2009). The exponential component in Eq. (2.2) is added to make more distant particles within the horizon of the particle $\mathbf{x}$ exert less influence on the particle $\mathbf{x}$ than the closer particles (Oterkus *et al.*, 2012; Kilic *et al.*, 2009; Weckner and Abeyaratne, 2005). To obtain a viscoelastic bond, a viscoelastic constitutive equation is inserted into the constant c_1 in the bond force equation

$$f(\boldsymbol{\eta},\boldsymbol{\xi}) = \frac{\boldsymbol{\xi}+\boldsymbol{\eta}}{|\boldsymbol{\xi}+\boldsymbol{\eta}|}\exp\Big[-\Big(\frac{|\boldsymbol{\xi}|}{l}\Big)^2\Big]c_1 s \tag{2.2}$$

3. Creep test material modelling

In this study, a nonlinear viscoelastic equation is used and inserted into the PD bond force equation. Nonlinearity of a viscoelastic material means that the strain of the material is nonlinear with the applied stress. There are several types of nonlinear viscoelasticity, namely nonlinearity at high temperatures, nonlinearity at large deformations, and material nonlinearity. Most polymers

are treated as nonlinear viscoelastic materials. In this work, nonlinearity at high temperatures is not considered because the temperature is constant. A potential nonlinear viscoelastic equation has been chosen and the formula is based on the thermodynamic theory of irreversible internal state variables (ISV).

The proposed viscoelastic formula can describe the four stages of creep deformation (Zhang *et al.*, 2014). The creep strain results from an internal structural adjustment, and the different creep stages are associated with different thermodynamic properties in terms of a flow potential function and energy dissipation rate. During the primary and secondary creep stages, the thermodynamic state of the material system tends to equilibrate spontaneously. These stages can be described by kinetic equations of ISVs, which can be derived by a single flow potential function in which the energy dissipation rate decreases monotonically with time. These stages can also be considered as "damage-free" stages. For the tertiary creep and fracture stages, multiple potentials are needed to describe the evolution of ISVs, so that the thermodynamic state of the material system tends to deviate from the steady strain rate state.

In Rice thermodynamic theory, there are three sets of dimensionless macroscale ISVs introduced i.e. γ, λ and χ. γ and λ are used to describe intrinsic structural changes in viscoelastic and viscoplastic processes respectively, and χ is used to account for the damage effect. The Rice irreversible ISV thermodynamics based on a constrained equilibrium state adopts that the state of a solid material at any given time can be described entirely by the stress $\boldsymbol{\sigma}$ or strain $\boldsymbol{\varepsilon}$, the temperature θ and a set of scalar internal state variables $\boldsymbol{\zeta}(\zeta_1, \zeta_2, \ldots, \zeta_n)$ that represent physical changes of microstructures of the material (Rice, 1971). These four variables are referred to as thermodynamic state variables. The specific free energy ϕ and specific complementary energy ψ are the main thermodynamic potential functions. They satisfy the Legendre transform (Rice, 1971; Yang *et al.*, 2005) as follows

$$\phi(\boldsymbol{\varepsilon}, \theta, \boldsymbol{\zeta}) + \psi(\boldsymbol{\sigma}, \theta, \boldsymbol{\zeta}) = \boldsymbol{\varepsilon} : \boldsymbol{\sigma} \tag{3.1}$$

Considering the neighbouring constrained equilibrium states, the equation corresponding to different sets of state variables can be written in thermostatic form as shown in the following equation

$$\delta\psi = \boldsymbol{\varepsilon} : \delta\boldsymbol{\sigma} + \theta\delta\overline{\eta} + \frac{1}{V} f_\alpha \delta\zeta_\alpha \tag{3.2}$$

The Gibbs free energy density φ has been presented in a paper (Schapery, 1999) and it is related to ϕ in the usual way

$$\varphi = \phi - \boldsymbol{\varepsilon} : \boldsymbol{\sigma} \tag{3.3}$$

Considering equation (3.1), we can obtain

$$\psi = -\varphi \tag{3.4}$$

According to the Gibbs free energy density function, the complementary energy density function ψ can be described as follows

$$\psi = \psi_e + A_2\gamma - \frac{1}{2}B\gamma^2 + P_\alpha\lambda_\alpha \tag{3.5}$$

where ψ_e, A, B and P_α may possibly be the state functions of stress $\boldsymbol{\sigma}$, temperature θ and damage χ. From the third component of Eq. (3.2), the thermodynamic force can be obtained from the complementary energy density by using the following function

$$f_\alpha = V\frac{\partial\psi}{\partial\zeta_\alpha} \tag{3.6}$$

This equation can be separated into three types of forced, i.e. the elastic force, plastic force and damage force as stated below in unit volume

$$\begin{aligned} f_e &= \frac{\partial \psi}{\partial \gamma} = A_2 - B\gamma \qquad f_p^{\alpha} = \frac{\partial \psi}{\partial \lambda_\alpha} = P_\alpha \qquad (\alpha = 1,2) \\ f_\chi &= \frac{\partial \psi}{\partial \chi} = \frac{\partial \psi_e}{\partial \chi} + \frac{\partial A_2}{\partial \chi}\gamma + \frac{\partial P_\alpha}{\partial \chi}\lambda_\alpha \end{aligned} \tag{3.7}$$

In Eq. $(3.7)_3$, the damage development under elastic and viscoelastic deformation can be neglected (Voyiadjis and Zolochevsky, 2000). Thus, Eq. $(3.7)_3$ can be simplified into

$$f_\chi = \frac{\partial \psi}{\partial \chi} = \frac{\partial P_\alpha}{\partial \chi}\lambda_\alpha \tag{3.8}$$

The strain equation can be constructed by considering the relationship between the strain and specific complementary energy as in Eq. $(3.9)_1$ and the relationship between the specific complementary energy and thermodynamic force as in Eq. $(3.9)_2$

$$\boldsymbol{\varepsilon} = \frac{\partial \psi}{\partial \boldsymbol{\sigma}} \qquad \psi(\boldsymbol{\sigma}, \theta, \boldsymbol{\zeta}) = \frac{1}{V} f_\beta \dot{\zeta}_\alpha \tag{3.9}$$

The strain equation can be expressed in terms of viscoelastic and viscoplastic strains as follows

$$\boldsymbol{\varepsilon} = \boldsymbol{\varepsilon}^{ve} + \boldsymbol{\varepsilon}^{vp} \tag{3.10}$$

where

$$\boldsymbol{\varepsilon}^{ve} = \frac{\partial A_2}{\partial \boldsymbol{\sigma}}\gamma + \mathbf{c} \qquad \boldsymbol{\varepsilon}^{vp} = \frac{\partial P_\alpha}{\partial \boldsymbol{\sigma}}\lambda_\alpha \tag{3.11}$$

The viscoelastic strain equation $\boldsymbol{\varepsilon}^{ve}$ includes the initial elastic strain and hardening effect. Since the hardening effect is also provided by the viscoplastic strain equation, $\dot{\boldsymbol{\varepsilon}}^{vp}$ as in Eq. (3.13), thus the viscoelastic strain equation, $\boldsymbol{\varepsilon}^{ve}$ can be replaced by the initial elastic strain, $\boldsymbol{\varepsilon}^{e}$ alone with E_e as the elastic modulus

$$\boldsymbol{\varepsilon}^{e} = \frac{\boldsymbol{\sigma}}{E_e} \tag{3.12}$$

The viscoplastic strain behavior can be described as follows

$$\dot{\boldsymbol{\varepsilon}}^{vp} = D_1[\dot{\boldsymbol{\lambda}}_1 + (1+\chi)\dot{\boldsymbol{\lambda}}_2 + b\dot{\boldsymbol{\lambda}}_2\dot{\chi}] \qquad D_1 = a_2 - \frac{1}{\sqrt{3}} \tag{3.13}$$

The parameter $\boldsymbol{\lambda}_1$ is used to describe the hardening effect and both $\boldsymbol{\lambda}_2$ and χ represent the softening effect and damage. The parameters $\boldsymbol{\lambda}_2$ and χ have a symbiotic relationship; χ has an evolution process only when $\boldsymbol{\lambda}_2$ develops.

In the one-dimensional form, λ_1, λ_2 and χ are given by ramp equations as shown below

$$\begin{aligned} \dot{\lambda}_1 &= \kappa_1 D_2 \Big\langle \sigma - \sigma_y - \frac{1}{D_2} k\lambda_1 \Big\rangle \qquad D_2 = \frac{1}{\sqrt{3}} - a_2 \\ \dot{\lambda}_2 &= \kappa_2 \Big\langle \frac{(1+b\chi)\sigma - \sigma_x}{\sigma_x} \Big\rangle^p \qquad \dot{\chi} = \kappa_3 \mathrm{e}^{\chi} \Big\langle \frac{b\lambda_2\sigma}{\sigma_x} \Big\rangle^2 \operatorname{sgn}(\dot{\lambda}_2) \end{aligned} \tag{3.14}$$

Both Macaulay's brackets in the equations for $\dot{\lambda}_1$ and $\dot{\lambda}_2$ are the ramp equation as shown below

$$\langle X \rangle = \begin{cases} X & X > 0 \\ 0 & X \leqslant 0 \end{cases} \tag{3.15}$$

and the ramp equation in equation for $\dot{\chi}$ is as following

$$\operatorname{sgn}(X) = \begin{cases} 1 & X > 0 \\ 0 & X = 0 \\ -1 & X < 0 \end{cases} \tag{3.16}$$

All the other unknowns, κ_1, κ_2, κ_3, D_2, k, a_2, b and p are parameters of the equation. σ_x is regarded as the mean internal stress (Aurbertin *et al.*, 1991). These creep parameters can be evaluated by fitting the numerical creep graph with the experimental creep data using the least square optimization method. Generally, the viscoelastic and viscoplastic deformations in the creep process can be distinguished in the unloading stage. During the unloading stage, the material with viscoelastic behavior returns to its original length while the material with viscoplastic behavior exhibits permanent deformation. When a viscoelastic material experiences prolonged creep deformation, viscoplastic behavior is initiated in the material once some limits are exceeded as stated in Eqs. (3.14).

The behavior of nonlinear strain as a function of the applied load can be incorporated into the viscoelastic equation by applying the Ramberg-Osgood equation (Irgens, 2008). This equation (Eq. (3.17)) was originally developed to describe the nonlinear relationship between stress and strain in materials near their yield point

$$\varepsilon = \frac{\sigma_0}{E} + \alpha_2 \frac{\sigma_0}{E} \Big(\frac{\sigma_0}{\sigma_y}\Big)^{n-1} \tag{3.17}$$

The parameter σ_0 is the applied stress, E is the Young modulus, σ_y is the yield strength, α_2 and n are temperature dependent material constants. The first and second term in the formula represent the elastic and plastic parts, respectively. It is assumed that the nonlinearity of strain with respect to the applied load occurs only in the secondary and tertiary creep stages, since the strain in the primary stage behaves linearly due to the low strain value. Therefore, the Ramberg-Osgood equation is added as a multiplier to the constant κ_2, which determines the strain rate of the secondary creep stage. The result is that only the strains at the secondary and tertiary stages are nonlinear with the applied load. The Ramberg-Osgood multiplier M is the nonlinear part in Eq. (3.17) as follows

$$M = 1 + \alpha_2 \Big(\frac{\sigma_0}{\sigma_y}\Big)^{n-1} \tag{3.18}$$

where the constant stress σ_0 and the Young modulus E are excluded. In equation (3.13), the parameter $\dot{\lambda}_1$ is a component of the viscoplastic strain rate $\dot{\varepsilon}^{vp}$ where it defines the secondary creep stage gradient. Since $\dot{\lambda}_1$ is directly proportional to the applied load as shown in Eq. $(3.14)_1$, the nonlinear relationship between the gradient of the secondary creep stage and the applied load in the nonlinear creep experiment can be a measure of the nonlinearity of the material. Therefore, the values of the parameters σ_y, α_2 and n in Eq. (3.17) can be obtained by the least square optimization method, by comparing Eq. (3.18) with the experimental curve of the gradients of the secondary creep stage as a function of the applied load.

The PD model with viscoelastic properties is obtained by substituting the viscoelastic creep equations as in Eqs. (3.10) to (3.18) into the material constant c_1 in the PD bond force in Eq. (2.2). The creep modulus function α, i.e., the strain-to-stress ratio function $(\boldsymbol{\varepsilon}/\boldsymbol{\sigma})$ of this nonlinear equation must be derived from the viscoelastic equation before substitution. However, since the nonlinear equation consists of several ramp functions, it is quite complex to derive the creep modulus function of this equation. For simplicity, this equation is calculated analytically to obtain a creep curve consisting of the primary, secondary, and tertiary stage. Then, the analytical creep curve is used as a reference for the numerical test by substituting the data of the curve

into the creep modulus α in the equation PD bond force as in Eq. (3.23). The time parameter in the viscoelastic equation is the real time t_R.

The critical strain is the value of the strain in the creep curve at which the transition from the secondary stage to the tertiary stage occurs. The value of the critical strain is determined by looking at the creep curve, where the value of the strain at which the strain deviates from the straight line of the secondary creep stage is the critical strain. In experiments, it is observed that at any value of the load, the critical strain is approximately the same (Drozdov, 2010). However, the viscoelastic equation has a disadvantage that the critical strains of the creep curves vary greatly for different values of applied loads. Alternatively, the reference creep curve is altered in which, initially, there is no tertiary stage behavior in the curve. The two damage equations, $\dot{\lambda}$ and $\dot{\chi}$ are initially disabled to remove the tertiary stage behavior. A single value for the critical strain is set, obtained from the experimental data. When the strain of a bond reaches the critical value, the damage equations ($\dot{\lambda}$ and $\dot{\chi}$) are activated to add the tertiary stage behavior.

In demonstrating fracture, the response function i.e., Eq. (2.2) can be modified by adding a history-dependent scalar-valued function μ (Silling and Askari, 2005) as follows

$$f(\boldsymbol{\eta},\boldsymbol{\xi}) = \frac{\boldsymbol{\xi}+\boldsymbol{\eta}}{|\boldsymbol{\xi}+\boldsymbol{\eta}|}\exp\Big[-\Big(\frac{|\boldsymbol{\xi}|}{l}\Big)^2\Big]c_1 s\mu(\xi,t) \tag{3.19}$$

where the function μ can be described as

$$\mu(\xi,t) = \begin{cases} 1 & \text{if } \ s(t',\xi) < s_0 \ \text{ for all } \ 0 < t' < t \\ 0 & \text{otherwise} \end{cases} \tag{3.20}$$

in which s_0 is the fracture stretch. The value of s_0 is determined considering the experimental data. During numerical calculation, the strain of each bond is continuously monitored. When the strain of a bond exceeds the value of s_0, the bond breaks and the two nodes connected by the bond no longer interact with each other. As can be seen in Fig. 2, the broken bond has the value μ equal to zero, and thus the bond force of the bond also becomes zero. As the number of broken bonds increases, a crack forms and eventually total fracture occurs.

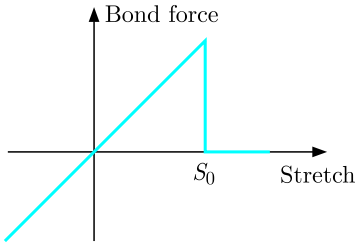

Fig. 2. The relationship between the bond force and stretch of a bond and the definition of fracture stretch s_0

The creep modulus α is introduced to put the nonlinear viscoelastic creep equation into the PD equation. The creep modulus describes the elongation of a viscoelastic material, and it is the ratio of strain to stress

$$\alpha(t_R) = \frac{\varepsilon}{\sigma} \tag{3.21}$$

In Eq. (3.21), the scalar bond force function as stated in Eq. (2.1) can be obtained by using the stress equation $\sigma = f/A$, where A is the cross-sectional area

$$\alpha(t_R) = \frac{\Delta l}{l_0}\frac{A}{f} \tag{3.22}$$

The elongation, Δl and the initial length l_0 in Eq. (3.22) are replaced with $|\boldsymbol{\eta}|$ and $|\boldsymbol{\xi}|$, respectively

$$\alpha(t_R) = \frac{|\boldsymbol{\eta}|}{|\boldsymbol{\xi}|}\frac{A}{f} \tag{3.23}$$

By arranging the bond force f as the subject of Eq. (3.23), the following scalar viscoelastic bond force equation is obtained

$$f(\boldsymbol{\eta}, \boldsymbol{\xi}, t_R) = \frac{|\boldsymbol{\eta}|A}{|\boldsymbol{\xi}|\alpha(t_R)} \tag{3.24}$$

In Eq. (2.2) $f = c_1 s$. Thus, the material constant c_1 for a time-dependent viscoelastic material is

$$c_1(t_R) = \frac{A}{\alpha(t_R)} \tag{3.25}$$

Substituting Eq. (3.25) into Eq. (2.2), a creep viscoelastic bond force equation derived

$$f(\boldsymbol{\eta}, \boldsymbol{\xi}) = \frac{\boldsymbol{\xi} + \boldsymbol{\eta}}{|\boldsymbol{\xi} + \boldsymbol{\eta}|} \exp\Big[-\Big(\frac{|\boldsymbol{\xi}|}{l}\Big)^2\Big]\frac{A}{\alpha(t_R)}s \tag{3.26}$$

The main difference between the elastic and viscoelastic PD bond force equations is the additional time parameter (real time t_R) in the creep modulus $\alpha(t_R)$. The value of A is unknown since there is no cross-sectional area between two nodes and, for simplicity, it is set to 1. Each bond or connection between two nodes acquires one bond force equation. In Eq. (2.1), the first component, i.e., the integral equation, sums all bond forces between the node $\mathbf{x}$ and other nodes within the horizon of the node $\mathbf{x}$.

The total bond force is then added with external forces $\mathbf{b}(\mathbf{x}, t)$ which include all-direction fixtures on the nodes at the bottom surface of the specimen and the upward loads on the nodes at the top surface of the specimen. The result of the addition is a resultant force of the node $\mathbf{F}_R$, which has the dimension of force per unit volume. Referring to Eq. (2.1), the acceleration of the node can be determined by dividing the resultant force by density of the material ρ as shown below

$$\frac{\partial^2 \mathbf{u}}{\partial t^2} = \frac{\mathbf{F}_R}{\rho} \tag{3.27}$$

It is in the nature of an integral-based numerical model such as the PD model that the simulation yields a dynamic result that fluctuates endlessly. In elastic peridyamic tests, the nodes fluctuate permanently, whereas in viscoelastic PD tests, the fluctuation of the nodes is damped by the existing dashpot properties. Since creep tests are in practice performed with static loading, a damping method is required to convert the dynamic data into static results. An effective method that provides this conversion is adaptive dynamic relaxation (ADR) (Hu *et al.*, 2014). The ADR method is used in this paper for each PD numerical test.

4. Experiment for validation

A creep experiment is performed to obtain creep data to be used as a reference for the numerical test. The material used for the experiments was polypropylene (PP). The size of the specimen conformed to ASTM D-638 and is 57 mm long, 13 mm wide, and was 3.2 mm thick. The specimens were manufactured using an injection molding machine, namely Battenfeld BA 250 CDC Injection Molding. The creep tests were performed using a Zwick Z100 universal machine. The values of the fixed loads applied to the specimens during the creep test were 12.5 MPa, 13 MPa, 13.5 MPa, 14 MPa and 14.5 MPa. The experimental procedure for the creep test was based on ASTM D2990.

5. Results and discussion

Prior to the numerical test, the values of the nonlinear viscoelastic parameters in scalar equations (3.14)-(3.18) were obtained from the optimization process by using the least square method with the experimental data as a reference. The values of the parameters are listed in Table 1.

Table 1. Optimized values of parameters in the viscoelastic constitutive equations

No.	Parameter	Optimized value	Unit	No.	Parameter	Optimized value	Unit
1	κ_1	0.04	$(\text{MPa}\cdot\text{s})^{-1}$	7	σ_x	-120	kPa
2	κ_2	0.10	10^{-6}s^{-1}	8	p	1.56	–
3	κ_3	0.014	10^{-5}s^{-1}	9	E_e	360	MPa
4	k	23.98	MPa	10	σ_y	0.529	MPa
5	a_2	0.201	–	11	α_2	7	–
6	b	0.248	–	12	n	15	–

The curves resulting from the creep experiment can be seen in Fig. 3. In Fig. 3, one can calculate the percentage difference between the numerical curve and the experimental curve. The difference is calculated by subtracting the experimental strain value with the numerical strain value at each time $t = 1, 2, 3, \ldots, t_{final}$. Then, each subtraction is divided by the experimental strain value at each time point to obtain the percentage difference at each time point in the curve. Then all the percentage differences are averaged to obtain the percentage difference for the whole curve. The percentage differences for all curves with different loadings are shown in Table 2. The overall percentage difference between the numerical and experimental data is 15.85%, which is the average value for the percentage differences of all five curves.

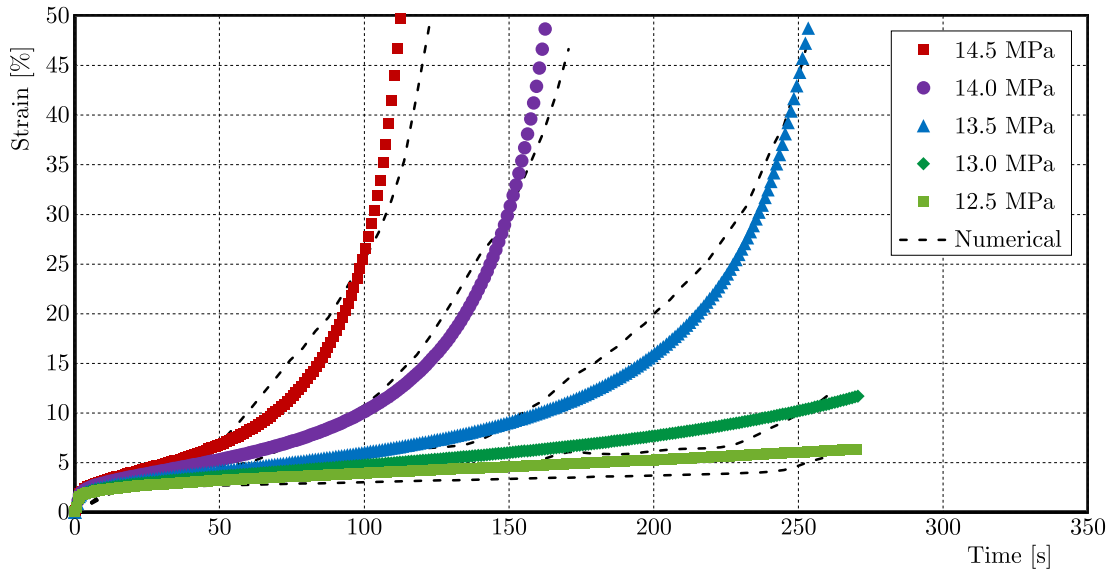

Fig. 3. Comparison between experimental (polypropylene) and PD numerical creep tests

The curve of the strain rate of the secondary stage characterises the nonlinearity of the creep behavior. The gradients of the secondary creep stage of all experimental and numerical curves in Fig. 3 are calculated, and the curve of the strain rate of the secondary stage for experimental and numerical data can be plotted as in Fig. 4. The average error between the strain rate of the secondary stage of experimental and numerical data is notable and is 21.83%.

Table 2. Percentage difference between numerical and experimental data for each curve

Creep stress [MPa]	Percentage of difference between num-exp [%]
12.5	20.65
13.0	17.11
13.5	14.20
14.0	11.52
14.5	15.77
Overall	15.85

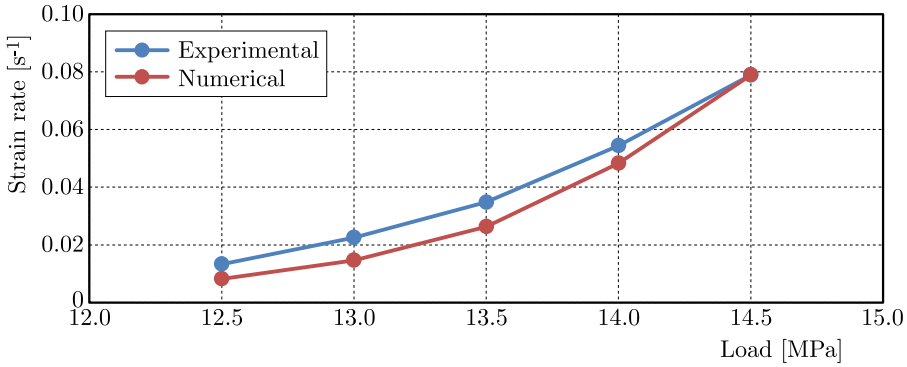

Fig. 4. Graph of the strain rate of the secondary creep stage against the applied load

There are several factors that cause significant values of the error. First, the numerical creep curves are bumpy, and the strain does not increase uniformly. This is because the number of bonds entering the tertiary creep stage does not increase smoothly, but instead increases with staircase behavior, as shown in Fig. 5a. This is due to the small number of nodes causing the lamination effect, in which all nodes within a layer perpendicular to the applied load tend to deform uniformly. Thus, when all nodes in the layer enter the tertiary stage simultaneously, the staircase effect occurs. Figure 5b shows the numerical creep curve generated by the same simulation that generates the curve in Fig. 5a. The creep curve shows an obviously uneven increase of the load. Because of the bumpy curves, the slope of the secondary creep stage cannot be accurately measured because it is unclear when the transition from the secondary stage to the tertiary stage occurs. Therefore, this is a factor in the remarkable error in the numerical gradients of the secondary creep stage as in Fig. 4.

Secondly, the primary creep stage has a relatively longer period in the numerical curves than in the experimental curves. The main reason for this effect is that the adaptive dynamic relaxation (ADR) method requires a long time before the strain reaches the equilibrium value. This problem can be solved by optimizing the ADR parameters to achieve faster convergence, and this solution requires a deeper understanding of the ADR method. Alternatively, the periods of the secondary and tertiary creep stages can be set longer to obtain a smaller ratio to the period of the primary creep phase, but this solution requires a longer simulation time.

Thirdly, the creep curves at a low load, i.e., at 12.5 MPa and 13 MPa, have a large error because as the value of strain decreases and approaches 1%, the behavior is transiting from nonlinear to linear viscoelasticity (Drozdov, 2010; Gao *et al.*, 2020). The nonlinear viscoelastic equation is not suitable for use at low strain values. The transition from linear to nonlinear viscoelasticity should be considered in the development of viscoelastic constitutive formulas in the future.

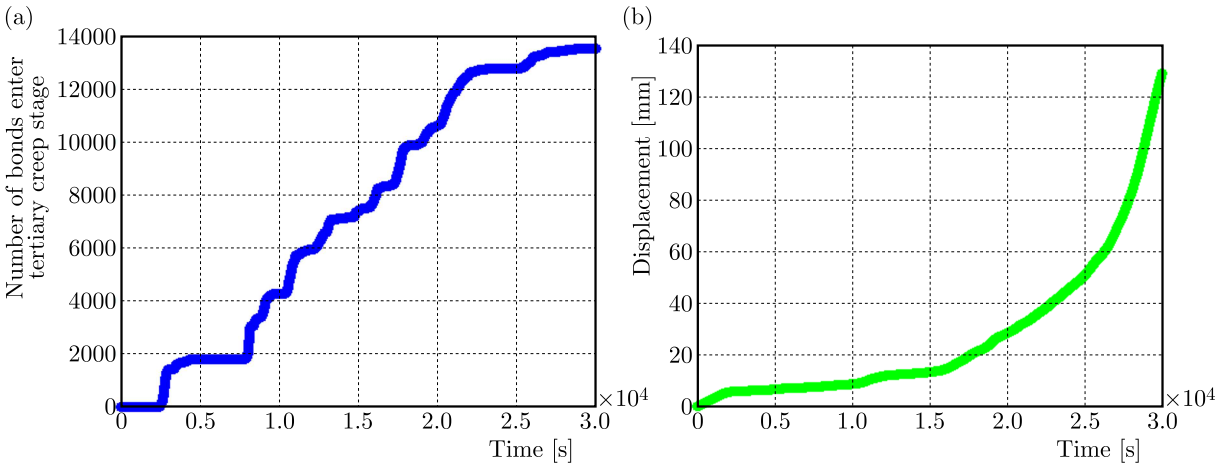

Fig. 5. (a) Number of bonds that enter the tertiary creep stage against time. (b) Numerical creep curve from the same simulation as the curve in (a)

The result for the creep fracture by using PD simulation with the ADR method is shown in Fig. 6b. A fractured polypropylene specimen from the same experiment that produces result shown in Fig. 3 is used for comparison with the fractured numerical specimen, and a photo of the specimen is shown in Fig. 6a. There is a number of similarities between the fractured numerical model and the fractured experimental specimen. Firstly, the shape of the necking has a close resemblance to the experimental specimen where the necking is large. Since the number of nodes in this model is less compared to the two-time method model, the roughness of the crack surface is unclear. However, comparing the upper surface with the crack surface, it can be seen that the crack surface is rougher than a normal surface. In both numerical and experimental specimens, the crack occurs on one side of the specimen and not in the centre.

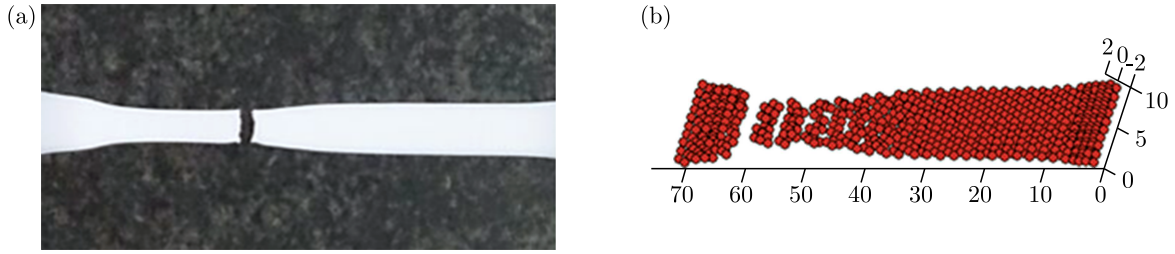

Fig. 6. (a) The shape of the fractured experimental specimen due to a creep test. (b) Numerical specimen shape after the creep test completed

Another problem related to fracture behavior is the location of the crack. From numerical creep tests using the two-time method and the ADR method, it appears that failure occurs near the point where the load is applied. This behavior is related to dynamic loading, when the load is suddenly applied to the specimen, causing a stress wave that begins at the point of loading and propagates across the specimen. This is undesirable behavior since the creep test is a static load test. This dynamic loading behavior is investigated by placing a notch in the centre of the specimen to see if the creep test failure occurs at the notch or not. The depth of the notch is varied to see how this variable affects the failure point.

Figure 7 shows the crack position for specimens with different notch depths subjected to a creep test at the beginning (left) and at the end (right) of the test. The four specimens have different values of notch depth, i.e., 3 nodes spacing, 5 nodes spacing, 7 nodes spacing and 9 nodes spacing. The width of the specimen is 10 node spacing. The load is applied to the top and bottom of the specimen. For all specimens, the fracture location is at the notched location,

except for the specimen with a notch depth of 3 nodes spacing, where the fracture occurs at the top of the specimen. In practice, the crack certainly occurs at the notch within the specimen due to stress concentration in the notch. The reason for the fracture behavior in specimens with a notch depth of 3 nodes spacing is the dynamic loading to which the specimen is subjected. The bonds at the ends of the specimen expand earlier than the bonds in the centre of the specimen, so the bonds at the ends break earlier than the bonds in the centre of the specimen. The solution to this problem is to create numerical simulations with static loading instead of dynamic loading.

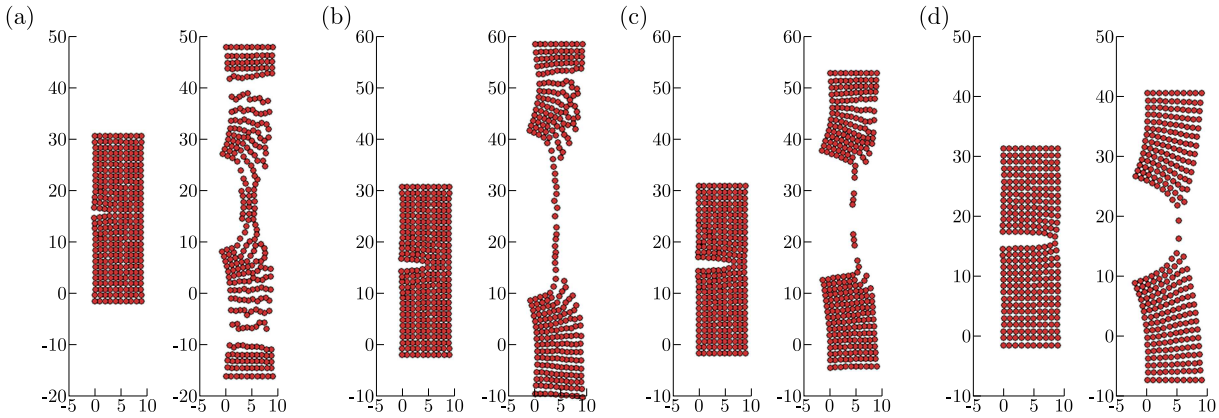

Fig. 7. Fracture location of numerical creep specimens with different notch depths

Additionally, to visualize the stress distribution of the PD numerical model as commonly practiced in conventional FEM, it can be achieved by considering the resultant force of the nodes within the numerical model. The resultant load is calculated by using Eq. (2.1). The stress in the model can be represented by the resultant load since there is no area parameter in the PD model. If the cross-sectional area of the bond is assumed to be equal to 1, the stress at a point is equal to the resultant load at the same point. Several examples of the resultant load variation in the PD numerical specimen are shown in Fig. 8. The colour of each node describes the value of the resultant load exerted on the node. Red means the highest range of the resultant load value, followed by orange, yellow, light green, dark green, light blue and dark blue.

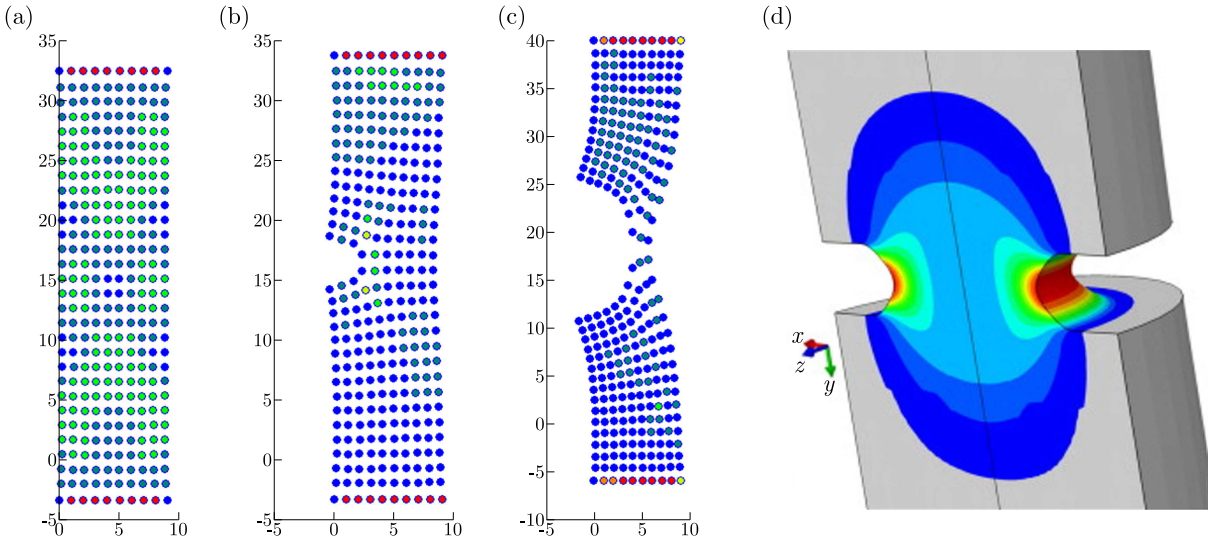

Fig. 8. Distribution of load in the creep test in: (a) specimen without notch, (b) specimen with 3 nodes length depth, (c) specimen with 7 nodes length depth. (d) Distribution of stress in the creep test in a FEM specimen (Goyal *et al.*, 2013)

In the first three diagrams in Fig. 8, the highest resultant load is experienced by the nodes at the top and bottom surfaces. This is due to the dynamic loading that is applied to the top and bottom surfaces of the specimen, and this behavior can be neglected. In Fig. 8a, the nodes that experience the resultant load in green range are separated in the middle of the specimen. This is again due to the dynamic loading that causes a rippling manner in the load distribution. In Fig. 8b and Fig. 8c, it is observed that the nodes near to the notches received a higher resultant load than the nodes in the other part of the specimens. This PD result is equivalent to the FEM stress distribution diagram as shown in Fig. 8d (Goyal *et al.*, 2013) where the stress concentration appears at the notch. In conclusion, these pictures of the distribution of resultant load in PD numerical specimens are equivalent to the FEM stress distribution diagram.

6. Conclusion

The PD simulation of viscoelastic creep behavior is validated by an adequate similarity in numerical-experimental data comparison. The numerical model is able to simulate four stages of creep i.e. the primary stage, secondary stage, tertiary stage and fracture. The numerical fractured specimens show apparent similarities with the experimental fractured specimen. The numerical test of specimens with a notch of different depth describes the unwanted dynamic loading in the PD simulation, since the creep test is a static loading test. In addition, the resultant load distribution diagram obtained from the PD creep test is equivalent to the conventional stress distribution diagram of the FEM. In summary, PD models on viscoelastic creep with rupture behavior are established, and these models can offer an improved fracture prediction in practice.

Acknowledgment

The authors gratefully acknowledge the supports provided by the Geran Putra IPM (Project code: GP-IPM/2018/9669600) awarded by Universiti Putra Malaysia.

References

1. Agwai A., Guven I., Madenci E., 2011, Crack propagation in multilayer thin-film structures of electronic packages using the peridynamic theory, *Microelectronics Reliability*, **51**, 12, 2298-2305
2. Aurbertin M., Gill D.E., Ladanyi B., 1991, An internal variable model for the creep of rocksalt, *Rock Mechanics and Rock Engineering*, **24**, 81-97
3. Brandner S., Becker T., Jekle M., 2019, Classification of starch-gluten networks into a viscoelastic liquid or solid, based on rheological aspects – A review, *International Journal of Biological Macromolecules*, **136**, 1018-1025
4. Drozdov A.D., 2010, Creep rupture and viscoelastoplasticity of polypropylene, *Engineering Fracture Mechanics*, **77**, 12, 2277-2293
5. Foster J.T., Silling S.A., Chen W.W., 2009, State based peridynamic modelling of dynamic fracture, *DYMAT 2009 – 9th International Conference on the Mechanical and Physical Behaviour of Materials under Dynamic Loading*, **2**, 1, 1529-1535
6. Gao L., Chen X., Gao H., Zhang S., 2010, Description of nonlinear viscoelastic behavior and creep-rupture time of anisotropic conductive film, *Materials Science and Engineering A*, **527**, 5115-5121
7. Goyal S., Laha K., Das C.R., Panneerselvi S., Mathew M.D., 2013, Finite element analysis of effect of triaxial state of stress on creep cavitation and rupture behaviour of 2.25Cr-1Mo steel, *International Journal of Mechanical Sciences*, **75**, 233-243
8. Ha Y.D., Bobaru F., 2011, Characteristics of dynamic brittle fracture captured with peridynamics, *Engineering Fracture Mechanics*, **78**, 6, 1156-1168

9. Hu W., Wang Y., Yu J., Yen C.-F., Bobaru F., 2013, Impact damage on a thin glass plate with a thin polycarbonate backing, *International Journal of Impact Engineering*, **62**, 152-165
10. Hu Y.I., Yu Y., Wang H., 2014, Peridynamic analytical method for progressive damage in notched composite laminates, *Composite Structures*, **108**, 1, 801-810
11. Irgens F., 2008, *Continuum Mechanics*, Springer-Verlag Berlin, Heilderberg
12. Kilic B., Agwai A., Madenci E., 2009, Peridynamic theory for progressive damage prediction in center-cracked composite laminates, *Composite Structures*, **90**, 2, 141-151
13. Kilic B., Madenci E., 2009, Structural stability and failure analysis using peridynamic theory, *International Journal of Non-Linear Mechanics*, **44**, 8, 845-854
14. Oterkus E., Madenci E., Weckner O., Silling S.A., Bogert P., Tessler A., 2012, Combined finite element and peridynamic analyses for predicting failure in a stiffened composite curved panel with a central slot, *Composite Structures*, **94**, 3, 839-850
15. Rice J.R., 1971, Inelastic constitutive relation for solids: an internal-variable theory and its application to metal plasticity, *Journal of the Mechanics and Physics of Solids*, **19**, 433-455
16. Schapery R.A., 1999, Nonlinear viscoelastic and viscoplastic constitutive equations with growing damage, *International Journal of Fracture*, **97**, 33-66
17. Silling S.A., 2000, Reformulation of elasticity theory for discontinuities and long-range forces, *Journal of the Mechanics and Physics of Solids*, **48**, 175-209
18. Silling S.A., Askari E., 2005, A meshfree method based on the peridynamic model of solid mechanics, *Computers and Structures*, **83**, 1526-1535
19. Voyiadjis G.Z., Zolochevsky A., 2000, Therodynamic modeling of creep damage in materials with different properties in tension and compression, *International Journal of Solids Structure*, **37**, 24, 3281-3303
20. Warren T.L., Silling S.A., Askari A., Weckner O., Epton M.A., Xu J., 2009, A non-ordinary state-based peridynamic method to model solid material deformation and fracture, *International Journal of Solids and Structures*, **46**, 5, 1186-1195
21. Weckner O., Abeyaratne R., 2005, The effect of long-range forces on the dynamics of a bar, *Journal of the Mechanics and Physics of Solids*, **53**, 3, 705-728
22. Xu Y., Yuan H., 2011, Applications of normal stress dominated cohesive zone models for mixed-mode crack simulation based on extended finite element methods, *Engineering Fracture Mechanics*, **78**, 3, 544-558
23. Yang Q., Chen X., Zhou W.Y., 2005, Microscopic thermodynamics basis of normality structure of inelastic constitutive relations, *Mechanics Research Communications*, **32**, 590-596
24. Zhang L., Liu Y., Yang Q., 2014, A creep model with damage based on internal variable theory and its fundamental properties, *Mechanics of Materials*, **78**, 44-55

Manuscript received October 27, 2021; accepted for print June 27, 2022